Relativistic effects in three-nucleon forces for nuclear matter and finite nuclei

A. H. Lippok and H. Müther
Institut für Theoretische Physik, Universität Tübingen, D-72076 Tübingen, Germany
(Received 14 July 2015; published 14 September 2015)

In order to simulate the relativistic effects of the Dirac-Brueckner-Hartree-Fock approach for finite nuclei, the part of the Urbana three-nucleon (3N) force is considered, which represents the enhancement of the small components of the Dirac spinors for the nucleons in the nuclear medium. This 3N force is included in a Brueckner-Hartree-Fock calculation with rearrangement terms using a realistic model for the NN interaction. The strength of the 3N force is adjusted to reproduce the empirical saturation point of nuclear matter and then used in corresponding studies of the closed shell nuclei ^{16}O and ^{40}Ca. Special attention is paid to a consistent treatment of the spectrum of particle states in the NN propagator of the Bethe-Goldstone equation.

DOI: 10.1103/PhysRevC.92.034312 PACS number(s): 21.60.Jz, 21.30.Fe, 21.65.−f, 26.60.Gj

I. INTRODUCTION

One of the main challenges of theoretical nuclear physics is the attempt to derive the bulk properties of nuclear systems, which includes the saturation properties of infinite nuclear matter and also the binding energies and size of finite nuclei, from a realistic model of the nucleon-nucleon (NN) interaction. In this context models of the NN interactions are called realistic if they have been determined to fit the experimental data for two nucleons, i.e., the NN scattering phase shifts and the data of the deuteron, with high accuracy. These so-called realistic NN interactions are in contrast to phenomenological or effective NN forces such as the Skyrme interactions [1,2] or relativistic mean field models [3], which are fitted to describe the bulk properties of nuclear systems using Hartree-Fock or mean-field approximations.

Examples of such realistic NN interactions are the one-boson-exchange (OBE) models of the Bonn (also Idaho) [4] group or the local interaction models of the Argonne or Urbana groups [5]. Rather sophisticated versions of these models have been developed, such as the CD-Bonn potential [6] and the Argonne V18 potential [5].

Although these potentials are "soft" compared to the hard-core potentials developed in the middle of the last century, they contain strong tensor- and short-range components, which make it inevitable to employ a calculation tool which treats correlations beyond the mean-field or Hartree-Fock approximation [7]. A typical example of such a many-body approach is the Brueckner-Hartree-Fock (BHF) approximation, which is based on the solution of two-nucleon scattering equation in the nuclear medium, leading to an energy- and density dependent effective interaction, the so-called G matrix.

Attempts have been made to compare this G matrix with the phenomenological models of a nuclear force as the Skyrme interaction mentioned above and identify the density dependence of the Skyrme interaction with the medium dependence of the G matrix [8,9].

The variation principle of Hartree-Fock calculations with density-dependent forces leads to rearrangement terms, which in the case of the Skyrme interaction are very important to obtain good agreement with the empirical data for nuclear matter and finite nuclei. Therefore also the BHF approximation has been extended to include such rearrangement terms. Accounting for the energy dependence of G this leads to the renormalized BHF (RBHF) approach [10] whereas the density dependent HF (DHF) approximation also accounts for the Pauli-rearrangement terms [9,11]. The inclusion of the rearrangement terms is not only justified to simulate the features contained in the effective theory, but, in contrast to BHF, the DHF approach fulfills the Hughenholtz–van Hove theorem due to the inclusion of the rearrangement terms [12].

The BHF approach using realistic NN interaction leads to a saturation point for nuclear matter. The saturation points calculated with various models for the realistic NN interaction form the so-called Coester band [7,13], which misses the empirical data in a significant way. Therefore many attempts have been made to explore various effects, which make the NN interaction in the nuclear medium different from the NN interaction in the vacuum. An example of such studies is the inclusion of subnucleonic degrees of freedom, e.g., in terms of intermediate excitations of the interacting nucleons to the $\Delta(3,3)$ resonance. Such mutual polarization effects should occur already in the interaction of two nucleons in the vacuum. In fact such processes with intermediate isobar excitations provide a substantial contribution to the medium range attraction of the NN interaction, which in the OBE model is described in terms of the exchange of a light scalar σ meson [14,15]. In the nuclear medium these attractive terms are quenched due to dispersive and Pauli effects, features which could be described in terms of a density-dependent NN force or a 3N interaction [16,17]. Such isobar effects turned out to be non-negligible; however, this did not cure the problem of the Coester band, i.e., they did not shift the saturation point calculated for nuclear matter to the empirical data.

Another form of medium dependence of the NN interaction has been supplied by the Dirac-Brueckner-Hartree-Fock (DBHF) approximation [18,19]. Here one considers the Dirac structure of the self-energy of the nucleon and accounts for the effect that the attractive scalar component of this self-energy yields Dirac spinors for the nucleons in the nuclear medium with an enhanced small component as compared to the corresponding spinor for a nucleon in the vacuum. Again this change of the Dirac spinors in the medium and the corresponding change for the matrix elements of meson exchange can be described either in terms of a medium-dependent

NN force or by means of a 3N force parameterized in theform of a Z diagram with 2σ exchange terms [20,21].

The DBHF approximation has been successful in the sense that it reproduced the empirical saturation point of nuclear matter without adjustment of any additional parameter [18,22–28]. Since, however, the consistent treatment of correlation and relativistic effects for finite systems is a rather involved problem, the full Dirac-Brueckner equations have not yet been solved for finite nuclei. In fact, Van Giai *et al.* [29] addressed this problem as one of the main open problems in nuclear physics. Different approximation schemes have been developed, which treat either the relativistic effects or the correlation effects in an approximate way.

The most popular approximation scheme is to analyze the DBHF calculations of infinite matter in terms of an effective field theory with meson-nucleon coupling constants depending on the nucleon density and perform relativistic mean field or relativistic Hartree-Fock calculations for finite nuclei using the semiphenomenological density functionals, which were adjusted to reproduce DBHF results for infinite matter [30,31]. For a recent discussion of such relativistic density functionals see [28] and references listed there. Such studies consider the relativistic features of DBHF explicitly, but ignore more or less the effects of correlations beyond the mean field approach. It has been pointed out that the rearrangement terms originating from the density dependence of the meson-nucleon coupling constants are very important to improve the description of finite nuclei [31].

In the present investigation we are going to discuss a different approximation scheme for the DBHF approach in finite nuclei. The focus is to consider the correlation effects in terms of a direct evaluation for finite nuclei and treat the Dirac effects in an approximate way. However, in contrast to the method developed in [32] the Dirac effects are not described in terms of a local density approximation but are simulated using a three-nucleon interaction.

Various attempts have been made to parametrize the 3N forces discussed so far in terms of a simple local 3N force. As an example we mention the Urbana force [33,34], which is composed of two terms,

$$V_{ijk} = A\, V_{ijk}^{2\pi} + U\, V_{ijk}^{R}. \tag{1}$$

The first part is from 2π exchange with an intermediate Δ excitation and may be considered to simulate the medium-dependent isobar effects discussed above. The second term is typically defined in terms of 2σ exchange and can be interpreted to simulate the effects of the Z diagram discussed above. This means the second term is thought to represent the relativistic effects of the DBHF approach [35]. Typically this 3N force is reduced to a density-dependent NN interaction, which is then added to the bare NN interaction (see, e.g., [36] and references therein) and the parameters A and U in Eq. (1) can be adjusted to reproduce the empirical saturation point for symmetric nuclear matter.

This scheme has been criticized by Hebeler and Schwenk [37] and later by Carbonne *et al.* [38] They argue that an expression for the total energy with kinetic energy t_i, 2N interaction V_{ij}, and 3N potential V_{ijk},

$$E = \sum_i t_i \rho_i + \frac{1}{2}\sum_{i,j} V_{ij}\rho_i\rho_j + \frac{1}{6}\sum_{i,j,k} V_{ikj}\rho_i\rho_k\rho_j\,, \tag{2}$$

leads to the single-particle energy

$$\varepsilon_i = t_i + \sum_j V_{ij}\rho_j + \frac{1}{2}\sum_{j,k} V_{ikj}\rho_k\rho_j\,, \tag{3}$$

which is different from the result that is obtained when the 3N force is added to the 2N interaction by

$$\frac{1}{2}V_{ij}^{\rm eff}(\rho) = \frac{1}{2}V_{ij} + \frac{1}{6}\sum_k V_{ikj}\rho_k\,. \tag{4}$$

This is of course true, and at first sight this would imply that the medium effects discussed above would lead to different results when they are treated in terms of a three-body force or considered as a density-dependent NN interaction. We note, however, that both approaches lead to the same result, if the single-particle energies are defined according to the Landau definition of the quasiparticle energy, i.e.,

$$\varepsilon_i = \frac{\partial}{\partial\rho_i}E(\rho), \tag{5}$$

which means that rearrangement terms due to the density dependence of $V^{\rm eff}$ are taken into account. With this inclusion the result is the independent on the treatment as a 3N term or a density-dependent 2N contribution.

In this investigation we will discuss Brueckner-Hartree-Fock kind of calculations for nuclear matter and finite nuclei based on a realistic NN interaction with inclusion of a three-nucleon force. Special attention will be paid to the rearrangement terms originating from the density dependence of the G matrix and the treatment of the 3N force in terms of a density-dependent 2N interaction. We will show that an adjustment of the constant U defining the relativistic three-body force in (1) is sufficient to obtain the empirical saturation point for symmetric nuclear matter. The same 3N force leads to a fair description also for the bulk properties of finite nuclei.

After this introduction we will discuss the Brueckner-Hartree-Fock approach with 3N forces and inclusion of rearrangement terms in Sec. II of this paper. The results for infinite matter and finite nuclei are discussed in Sec. III. Special attention will be paid to the treatment of the 3N force in finite nuclei and the description of the particle state spectrum in the Bethe-Goldstone equation. The main results and conclusions are summarized in Sec. IV.

II. BRUECKNER HARTREE FOCK APPROACH AND REARRANGEMENT TERMS

A. Nuclear matter and finite nuclei

The Brueckner Hartree Fock (BHF) approach can be defined in terms of three central equations. The first one of these equations is the Bethe-Goldstone equation

$$G(\omega) = V + V\frac{\hat{Q}}{\omega - \hat{H}_0}G \tag{6}$$

defining the so-called G matrix in terms of the free-space NN interaction V. Replacing the Pauli operator $\hat{Q}$—which forbids the scattering of the interacting nucleons into statesthat are below the Fermi energy and therefore occupied by other nucleons—with the unit operator and the energy denominator $\omega - \hat{H}_0$ with the difference of kinetic energies of free nucleons, the G matrix turns into the Lippman-Schwinger equation defining the scattering matrix T for two nucleons in the vacuum. Therefore the Bethe-Goldstone equation can be interpreted as the solution of the problem of two nucleons interacting in the nuclear medium and the G matrix can be understood as the effective interaction of two nucleons, which accounts for correlation between the interacting nucleons. The single-particle energies are then defined within the standard BHF approach using the Hartree-Fock expression in terms of the G-matrix interaction:

$$\varepsilon_i^{\mathrm{BHF}} = \langle i|\hat{t}|i\rangle + \sum_j \langle ij|G(\omega = \varepsilon_i + \varepsilon_j)|ij\rangle \rho_j \,. \tag{7}$$

The single-particle density ρ_j is diagonal in the basis of Hartree-Fock states

$$\langle k|\hat{\rho}|j\rangle = \rho_j \delta_{jk} \,,$$

and the diagonal elements ρ_j take the values 1 for occupied hole states with energies ε_j below the Fermi energy and 0 for the particle states above the Fermi level. In the case of finite nuclei these Hartree Fock states have to be determined as the eigenstates of the BHF single-particle Hamiltonian, which corresponds to the single-particle energies defined in Eq. (7). In the case of infinite nuclear matter these single-particle states are plane waves due to the symmetry of the system under translational transformation. Note, however, that also in the case of infinite matter a self-consistent solution of the Bethe-Goldstone equation (6) and the evaluation of the single-particle energies according Eq. (7) are required to determine the starting energy ω according to the Bethe-Brandow-Petchek theorem.

After solving Eqs. (6) and (7) in a self-consistent way one can evaluate the total energy as

$$E = \sum_i \langle i|\hat{t}|i\rangle \rho_i + \frac{1}{2}\sum_{ij} \langle ij|G(\omega = \varepsilon_i + \varepsilon_j)|ij\rangle \rho_j \rho_i \,, \tag{8}$$

which is the third of the three equations to define the BHF approximation. Note that using the BHF definition of the single-particle energies (7) the corresponding expression for the total energy leads to Koltuns sum rule [39]

$$E^{\mathrm{BHF}} = \sum_i \frac{1}{2}\left(\langle i|\hat{t}|i\rangle + \varepsilon_i^{\mathrm{BHF}}\right)\rho_i \,. \tag{9}$$

The definition of the single-particle energies for the intermediate particle states, i.e., the definition of the operator H_0 in the propagator of the Bethe-Goldstone equation (6) has been discussed for many years. It has been shown by Song *et al.* [40] that the contribution from three-body correlations is minimized in nuclear matter with the so-called continuous prescription [41], which means that the single-particle energies for the states above the Fermi level are calculated in the same way as those for the hole states below. As will be discussed below, we will try to adopt this prescription in our calculations. Since it is very elaborate to evaluate the single-particle energies for all states in finite nuclei, we will approximate the Hamiltonian for the two-particle states in this case by

$$\hat{H}_0 = \hat{Q}(\hat{t}_1 + \hat{t}_2)\hat{Q} - 2C, \tag{10}$$

which is the operator of the kinetic energy of the interacting particles restricted to the states above the Fermi energy. A constant C is introduced to make the spectrum "continuous" across the Fermi energy. Appropriate values will be discussed below.

Another rather technical obstacle for the solution of the Bethe-Goldstone equation (6) is the definition of the Pauli operator $\hat{Q}$. This Pauli operator is easily defined for nuclear matter using the rest frame of the nuclear matter system by

$$\hat{Q}|\vec{k}_1, \vec{k}_2\rangle = \begin{cases} |\vec{k}_1, \vec{k}_2\rangle & \text{for } |\vec{k}_1| > k_F \text{ and } |\vec{k}_2| > k_F \,, \\ 0 & \text{else,} \end{cases}$$

with $\vec{k}_i$ denoting the momenta of the interacting nucleons and the Fermi momentum k_F. The Bethe-Goldstone equation, however, is more easily solved in the center-of-mass frame of the interacting nucleon, as the momentum of the center of mass is conserved and the relative momentum can be expanded in a partial wave basis. Therefore one typically employs the so-called angle-average approximation for the Pauli operator and approximates the single-particle spectrum by a quadratic form

$$\varepsilon(\vec{k}) = \frac{\vec{k}^2}{2m^*} + C^* \tag{11}$$

with an effective mass m^* and a constant C^* fitted to describe the single-particle spectrum for the states below the Fermi momentum. Using these approximations, the Bethe-Goldstone equation can be solved separately in each partial wave, which reduces the numerical effort drastically. Methods have been developed to treat the Pauli operator and the single-particle spectrum without these approximations [42,43] and it has been shown that the angle average in the Pauli operator is a reasonable approximation, while the parametrization of the single-particle spectrum according to Eq. (11) can lead to considerable differences, as we will also discuss below.

The problem of a precise treatment of the two-particle propagator is even more pronounced in calculation of finite nuclei, as the single-particle states are only defined after the corresponding Hartree-Fock equations have been solved. Since we are using the simple parametrization of Eq. (10) for the single-particle spectrum, we avoid a precise treatment for the Pauli operator (see, e.g., [9]) and use the so-called angle average for finite nuclei [44,45] for a basis of oscillator states, which is appropriate for the nucleus under consideration.

The single-particle states $|i,lj\rangle$ states are expanded in the very same oscillator basis $|n,lj\rangle_{\mathrm{HO}}$

$$|i,lj\rangle = \sum_n c_{n,i}^{lj} |n,lj\rangle_{\mathrm{HO}} \,, \tag{12}$$

assuming spherical symmetry of the states for the closed-shell nuclei considered. The quantum numbers l and j refer to the orbital and total angular momenta of the single-particle states and the projection quantum numbers for the angular momentum are dropped. An attempt is made to optimize the oscillator basis in the sense that the oscillator parameter is chosen such that the corresponding expansion coefficients $c^{lj}_{n,i}$ are close to 1 for all occupied single-particle states. In this way it is typically sufficient to restrict the expansion in Eq. (12) to radial quantum numbers $0 \leqslant n \leqslant 4$.

The expansion coefficients $c^{lj}_{n,i}$ can then be determined by solving the BHF equations, which are given in the oscillator representation by

$$\sum_n \{\langle n',lj|\hat{t} + U^{\rm BHF}|n,lj\rangle_{\rm HO} + \} c^{lj}_{ni} = \varepsilon_i c^{lj}_{n'i}\,, \qquad (13)$$

with $\langle n',lj|\hat{t}|n,lj\rangle_{\rm HO}$ the matrix elements for the kinetic energy in the basis of oscillator states and the corresponding matrix elements for the BHF single-particle potential, which can be calculated as

$$\begin{aligned}&\langle n',lj|U^{\rm BHF}|n,lj\rangle_{\rm HO}\\ &= \sum_{kl'j'mm'J} \frac{2J+1}{2j+1} \langle n',lj,m,'l'j'|G|n,lj,m,l'j'\rangle^J_{\rm HO}\\ &\quad \times \rho^{l'j'}_k c^{l'j'}_{m'k} c^{l'j'}_{mk}\,, \end{aligned} \qquad (14)$$

with the anti-symmetrized matrix-elements of the G matrix $\langle n',lj,m,'l'j'|G|n,lj,m,l'j'\rangle^J_{\rm HO}$ in the basis of two-nucleon oscillator states coupled to total angular momentum J. The nonlinear equations (13) and (14) are solved in an iterative way to obtain self-consistent solutions for the expansion coefficients c^{lj}_{ni} as well as single-particle energies ε_i of the BHF single-particle states.

The effects of the 3N interaction are taken into account using a density-dependent 2N interaction as indicated in Eq. (4) Note, however, that the weighting coefficients of this density-dependent 2N interaction have been adjusted to obtain the correct expressions for the total energy and single-particle energies as presented in Eqs. (2) and (3), respectively.

B. Rearrangement terms

The BHF approximation, which has briefly been sketched in the preceding subsection, corresponds to a Hartree-Fock calculation, replacing the two-particle interaction by the corresponding G matrix. The G matrix, however, must be understood as an effective interaction, due to its dependence on the starting energy ω and the Pauli operator, depends on the density operator of the system considered. Therefore the BHF definition of the single-particle energy does not obey the Landau definition of the quasiparticle energy in (5). In fact, applying the Landau prescription to the energy functional (8) one obtains the BHF terms of (7) plus two additional terms, the starting energy rearrangement term ΔU^{ω}_i and the Pauli rearrangement term ΔU^{Q}_i, which are due to the dependence of G on starting energy ω and Pauli operator Q.

The starting energy rearrangement term can be written

$$\begin{aligned}\Delta U^{\omega}_i &= \sum_{j,k} \rho_j \rho_k \langle j,k|\frac{\partial G}{\partial \omega}|j,k\rangle \frac{\partial \varepsilon_j}{\partial \rho_i}\\ &= \sum_{j,k} \rho_j \rho_k \langle j,k|\frac{\partial G}{\partial \omega}|j,k\rangle \langle i,j|G|i,j\rangle. \end{aligned} \qquad (15)$$

The second line of this equation is obtained by substituting ε_j in the first line by the corresponding BHF definition of the single-particle energy. This may be considered as an approximative treatment of the starting energy rearrangement term. In principle one may prefer an approach in which the single-particle energy ε_j in the first line of Eq. (15) is replaced by the complete definition of the single-particle energy including starting-energy- and Pauli-rearrangement terms as well as effects arising from the 3N force. This leads to a summation of a large class of terms in the definition of the single-particle potential and has been discussed e.g. in [46]. The contributions of these higher-order terms, however, is small, therefore will be ignored in the present work. Treating the rearrangement terms in leading order only, we also ensure that the effect of the 3N force is identical if its treated as a 3N force or simulated in terms of a density-dependent 2N force with inclusion of the corresponding rearrangement term [see discussion of Eqs. (2) to (4) above].

Note that adding ΔU^{ω}_i to the BHF definition of the single-particle energy leads to

$$\varepsilon^{\rm RBHF}_i = \varepsilon_i + \Delta U^{\omega}_i \qquad (16)$$

$$= \langle i|\hat{t}|i\rangle + \sum_j \langle ij|G(\omega = \varepsilon_i + \varepsilon_j)|ij\rangle P_j\,, \qquad (17)$$

which means that we have replaced the single-particle density ρ_j in Eq. (7) by

$$P_j = \rho_j \left[1 + \sum_k \rho_k \langle j,k|\frac{\partial G}{\partial \omega}|j,k\rangle\right]. \qquad (18)$$

This expression for P_j typically yields values of the order of 0.8–0.9 and is often interpreted as a partial occupation of states j below the Fermi energy. The approximation (16) represents the leading terms of the so-called renormalized BHF approach (RBHF) [8,9]. Therefore we will use this name also in the following. Note that the Koltun sum rule of (9) cannot be used any longer to evaluate the total energy (8) using the RBHF definition of the single-particle energy.

The Pauli rearrangement term can be written as

$$\Delta U^{Q}_i = -\sum_{j,k,l} \rho_j \rho_k |\langle j,k|G|i,l\rangle|^2 \frac{1-\rho_l}{\varepsilon_j + \varepsilon_k - \varepsilon_i - \varepsilon_l}, \qquad (19)$$

and corresponds to the term of second order in G in the hole-line expansion of the self-energy. Calculations including Pauli- and starting energy rearrangement terms will be denoted as density-dependent Hartree-Fock calculations (DHF) and employ single-particle energies of the form

$$\varepsilon^{\rm DHF}_i = \varepsilon_i + \Delta U^{\omega}_i + \Delta U^{Q}_i \qquad (20)$$

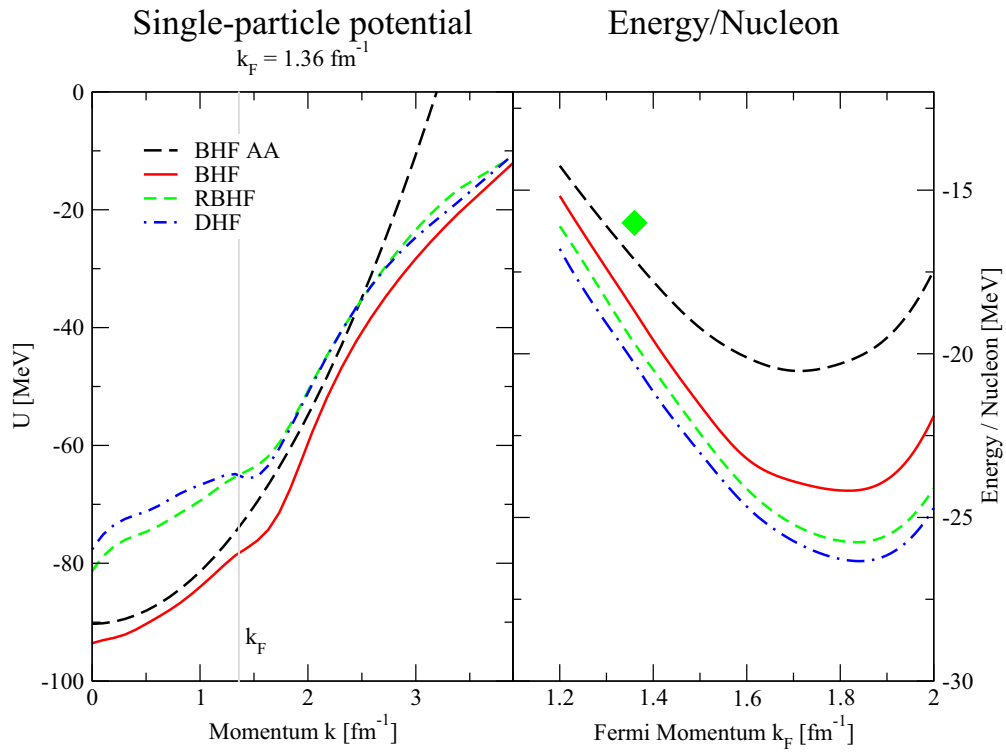

FIG. 1. (Color online) Results for symmetric nuclear matter calculations using the *pn* interaction of the CD-Bonn potential. The left panel presents results for the single-particle potential $U(k)$ assuming a Fermi momentum k_F of 1.36 fm^{-1}, which corresponds to the empirical saturation densities. Results are displayed for the BHF approximation using the angle -average in the Bethe-Goldstone equation (BHF AA) and BHF, RBHF [see Eq. (16)] and DHF [see Eq. (20)] calculations solving the Bethe-Goldstone equation without this approximation. The right panel shows the corresponding results for the energy per nucleon calculated at various Fermi momenta.

III. RESULTS

A. Nuclear matter

All the calculations presented here have been performed using the proton-neutron part of the charge-dependent Bonn (CD-Bonn) interaction, which has been defined and adjusted to the two-nucleon data by Machleidt, Sammarruca, and Song [6].

Results of conventional BHF calculations for symmetric nuclear matter, using the angle-average approximation for the Pauli operator and the parametrization of the single-particle potential using the quadratic form of Eq. (11) are presented by the dashed line, labeled BHF AA, in Fig. 1. The single-particle potential, which is displayed in the left panel of this figure for a Fermi momentum k_F of 1.36 fm^{-1}, which corresponds to the empirical saturation density, reflects the quadratic parametrization, which is adjusted to reproduce the BHF single-particle potential $U(k)$ for momenta k below the Fermi momentum and extended to momenta above k_F.

The calculated binding energy per nucleon of such BHF AA calculations, shown in the right panel of Fig. 1, yield a minimum, representing the prediction for the saturation point, at about twice the empirical saturation density and an energy of around -20 MeV, which is much more attractive than the empirical value of -16 MeV.

The consistent treatment of the two-particle propagator in the Bethe-Goldstone equation (6), avoiding the angle average of the Pauli operator and using a consistent single-particle spectrum, leads to quite different results as can be observed from a comparison of the BHF results, presented by the red solid curves in Fig. 1 and the BHF AA results. As it has been discussed by Schiller *et al.* [42], these differences can mainly be attributed to the definition of the single-particle potential. As can be seen from the left panel of Fig. 1, the single-particle energies used to define the propagator of the Bethe-Goldstone equation are quite similar for momenta below k_F. For the particle states with momenta above k_F, however, the calculated BHF energies are more attractive than described by the quadratic parametrization of the BHF AA approach.

The corresponding differences in the two-particle propagator lead to matrix elements of G, which are in general more attractive in the BHF than in the BHF AA approach, which leads to more binding energy in the former as compared to the latter calculation. This can be seen from the energy as a function of density curves, presented in the right panel of Fig. 1. The BHF calculations yield a saturation point with even larger binding energy (-24 MeV) than the BHF AA approach at a larger saturation density.

Figure 1 also provides the relevant information about the effects of the rearrangement terms in the definition of the single-particle potential in Eqs. (16) and (20). The dominant contribution arises from the starting energy rearrangement term, ΔU_i^{ω}, which is taken into account using the RBHF approximation. As expected from the representation of the

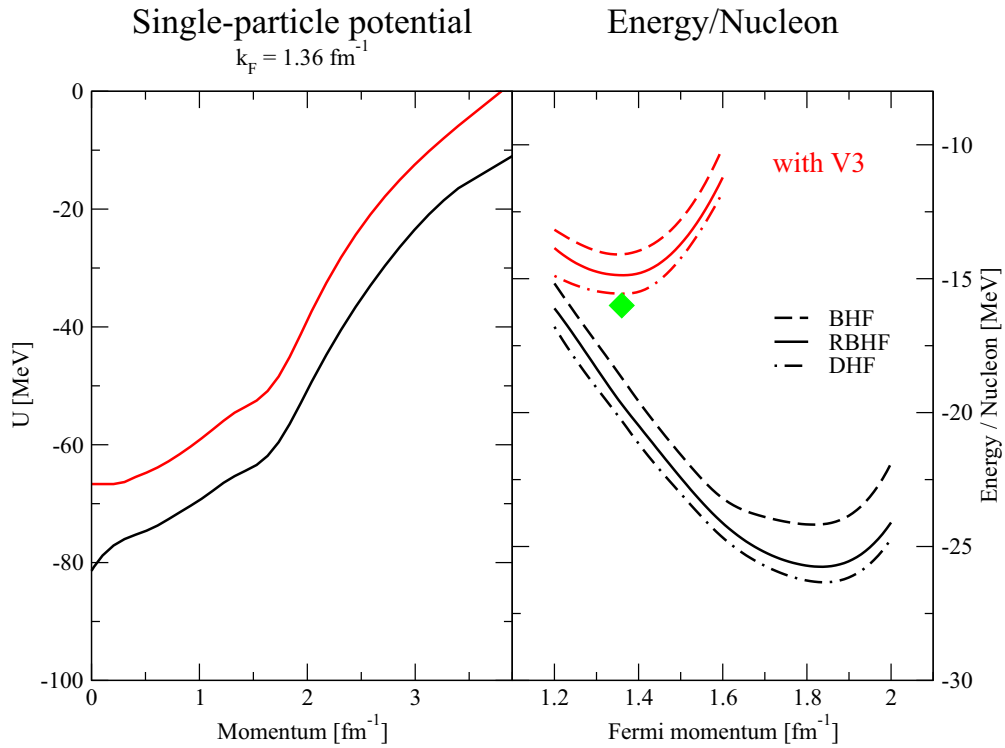

FIG. 2. (Color online) Results for symmetric nuclear matter calculations using the CD-Bonn potential with (red curves) and without inclusion (black curves) of the 3N potential. The left panel presents results for the single-particle potential $U(k)$ assuming a Fermi momentum k_F of 1.36 fm^{-1} for the RBHF approximation. The right panel shows results for the energy per nucleon calculated at various Fermi momenta for the of BHF, RBHF, and DHF approximations.

RBHF energies in terms of the partial occupation probabilities defined in (18), these are less bound than the corresponding BHF single-particle energies. This effect is more pronounced for the states with momenta below k_F than for the particle states above the Fermi momentum. This enhances the calculated binding energy even more, leading to a saturation point with an energy per nucleon of less than -25 MeV at a Fermi momentum of k_F of 1.8 fm^{-1}, which corresponds to a saturation density 2.3 times the empirical value.

The Pauli rearrangement term, which is also included in the DHF approximation, has a small effect. Its main effect in the single-particle potential is concentrated at momenta around the Fermi momentum, where it leads to a reduction of the momentum dependence of $U(k)$. This corresponds to the enhancement of the effective mass m^* to the bare mass m, as has already been discussed, e.g., by Mahaux and Sartor [47] and in [48]. The weak contribution of the Pauli rearrangement effect is also reflected in the small difference of the energies calculated in the DHF as compared to RBHF approximation. It is worth noting that the qualitative features of the Pauli rearrangement terms correspond to the effects the M_2 contributions of the extended BHF (EBHF) approximation discussed by Zuo *et al.* in [11,49]. The absolute effect of the M_2 term, as displayed, e.g., in Fig. 1 of [49], however, seems to be larger than the difference between DHF and RBHF presented here. This may be due to the fact that the CD-Bonn interaction, which is considered in the present calculation is softer than the Argonne interaction used by Zuo *et al.* Also note that the Pauli operator has been treated in [11,49] using the angle-average approximation.

All the calculations discussed so far have been performed assuming just a realistic two-nucleon interaction only—here the CD-Bonn interaction—and we find that the results of the calculated saturation points are part of the so-called Coester band [7,13]. This is true for the BHF approach, and the rearrangement terms just provide a shift along this Coester band. As it is one of the main goals of this investigation to simulate the relativistic effects in terms of a 3N potential, we considered the 3N part of the Urbana interaction model [33,34], fixing the parameter A in Eq. (1) to be equal to zero and adjusting the parameter U, the strength parameter for the term to simulate the change of the Dirac spinors in the medium, to reproduce the empirical saturation point. We did not aim at a high-precision fit, but just tried to obtain results close to the experimental data.

Results of such calculations are displayed in Fig. 2. It is worth noting that we can obtain a good description of the empirical saturation point by adjusting only one parameter, whereas most of the other attempts employ consider a three-nucleon interaction with two or more parameters for a corresponding fit.

The 3N term V_{ijk}^{R} [see Eq. (1)], which we consider in our studies, is of shorter range than the corresponding 2π exchange term, $V_{ijk}^{2\pi}$. This may be the reason that the 3N term essentially provides a repulsive shift in the single-particle potential $U(k)$ with almost no momentum dependence (see the example in the

TABLE I. Results for ^{16}O using BHF and RBHF approximations without (NN only) and with inclusion of the 3N interaction (with 3N) and with 3N interaction in the global density approximation (with 3N GD). Values of single-particle energies (ε) occupation probabilities [P, see Eq. (18)] are listed for the occupied states as well as the energy per nucleon (E/A) and the radius of the charge distribution (R_c). The Pauli operator in the Bethe-Goldstone equation has been defined in terms of oscillator function using an oscillator parameter $b = 1.767$ fm and $C = 5$ MeV has been used to define the single-particle energies in Eq. (10).

^{16}O	NN only			with 3N			with 3N GD			Expt. ε
	BHF	RBHF		BHF	RBHF		BHF	RBHF		
	ε (MeV)	ε (MeV)	P	ε (MeV)	ε (MeV)	P	ε (MeV)	ε (MeV)	P	
	Protons									
$s_{1/2}$	−58.19	−48.69	0.892	−44.76	−36.88	0.917	−41.59	−32.89	0.903	-44 ± 7
$p_{3/2}$	−27.05	−20.93	0.897	−20.22	−14.82	0.840	−17.64	−12.11	0.797	−18.45
$p_{1/2}$	−20.02	−16.25	0.871	−16.50	−12.27	0.824	−14.20	−9.80	0.792	−12.12
	Neutrons									
$s_{1/2}$	−62.22	−52.07	0.892	−48.36	−39.67	0.918	−45.12	−35.58	0.907	−47
$p_{3/2}$	−30.98	−24.19	0.901	−23.71	−17.60	0.846	−21.02	−14.69	0.802	−21.84
$p_{1/2}$	−23.83	−19.44	0.875	−20.00	−15.05	0.829	−17.61	−12.36	0.795	−15.66
E/A (MeV)	−6.08	−6.57		−4.61	−5.22		−3.93	−4.81		−7.98
R_c (fm)	2.35	2.45		2.59	2.66		2.64	2.72		2.74

left panel of Fig. 2). So we do not obtain the strong momentum dependence which has been observed by Zuo *et al.* [50].

B. Finite nuclei

The focus of the present investigation is to see if a BHF calculation with a parametrization of the Dirac effects in terms of a 3N interaction can provide a good description for the saturation point of nuclear matter as well as the bulk properties of finite nuclei. For that purpose we performed BHF and RBHF calculations for the closed shell nuclei ^{16}O and ^{40}Ca using the same 2N and 3N interactions as just described for nuclear matter.

Results of BHF calculations of ^{16}O using just the CD-Bonn potential are presented in Table I. One finds that the calculated energy per nucleon (−6.08 MeV) is less attractive as compared to the experimental value (−7.98 MeV) and the calculated radius for the charge distribution, R_c, is much lower (2.35 fm) than the empirical value of 2.74 fm. In order to visualize this result for the "saturation point" for ^{16}O in a way that corresponds to the plot for nuclear matter as given, e.g., in the right panel of Fig. 2, we indicated this result in the energy versus the inverse of the radius of the charge distribution by a red dot in Fig. 3. In fact, it is the upper of the two red dots, connected by a solid line in the left panel of this figure.

Compared to the empirical data, represented by a green diamond, we observe a situation that is quite different for ^{16}O than for nuclear matter (see Fig. 2). In both cases the BHF calculations yield value for k_F or $1/R_c$ that are too large as compared to experiment, which implies that the average density calculated for the nuclear systems is too large. With respect to the energy per nucleon, however, the BHF calculations provide too much energy in nuclear matter and too little for the finite nucleus. Therefore, in order to improve the comparison with experiment, the inclusion of the same 3N force must provide attraction in finite nuclei and repulsion in infinite matter and reduce the calculated saturation density in both cases.

The inclusion of rearrangement terms going from the BHF to the RBHF approach yields occupation probabilities P_i of the order of 0.8 to 0.9 as shown in Table I. From Eq. (16) it is obvious that this leads to less attractive single-particle energies in RBHF as compared to the BHF approach. The smaller attraction of the single-particle potential is reflected in a larger radius of the charge distribution. On the other hand the less attractive single-particle energies yield less attractive starting energies ω in the Bethe-Goldstone equation, which leads to more attractive matrix elements of the G matrix and results in a more attractive energy per nucleon. This means that the inclusion of rearrangement terms shifts both, the energy per nucleon and the radius of the charge distribution closer to the experiment. As one can see from Table I and Fig. 3, this effect is too small to provide a satisfying agreement.

The study of nuclear matter discussed above already showed that the results of BHF kind of calculations are rather sensitive to a consistent treatment of the two-particle propagator in the Bethe-Goldstone equation. The treatment of the particle-state spectrum in particular requires special attention. The same is of course also to be expected for finite nuclei. As discussed in the previous section, we approximate the Pauli operator Q in the Bethe-Goldstone equation (6) by a corresponding operator assuming oscillator states with an oscillator parameter $b = 1.76$ fm and $b = 2$ fm in the cases of ^{16}O and ^{40}Ca, respectively. The spectrum of the particle states, denoted by H_0 in Eq. (6), is represented by the simple parametrization of (10), trying to adjust the constant C in such a way that the resulting spectrum roughly matches the calculated single-particle energies. All the results displayed in Table I have been evaluated with $C = 5$ MeV. This choice is in line with an old coupled cluster calculation by Zabolitzky [51] demonstrating that such a choice would minimize the effects of 3N correlations in calculations of ^{16}O. On the other hand, the QTQ spectrum in the single-particle space considered yields

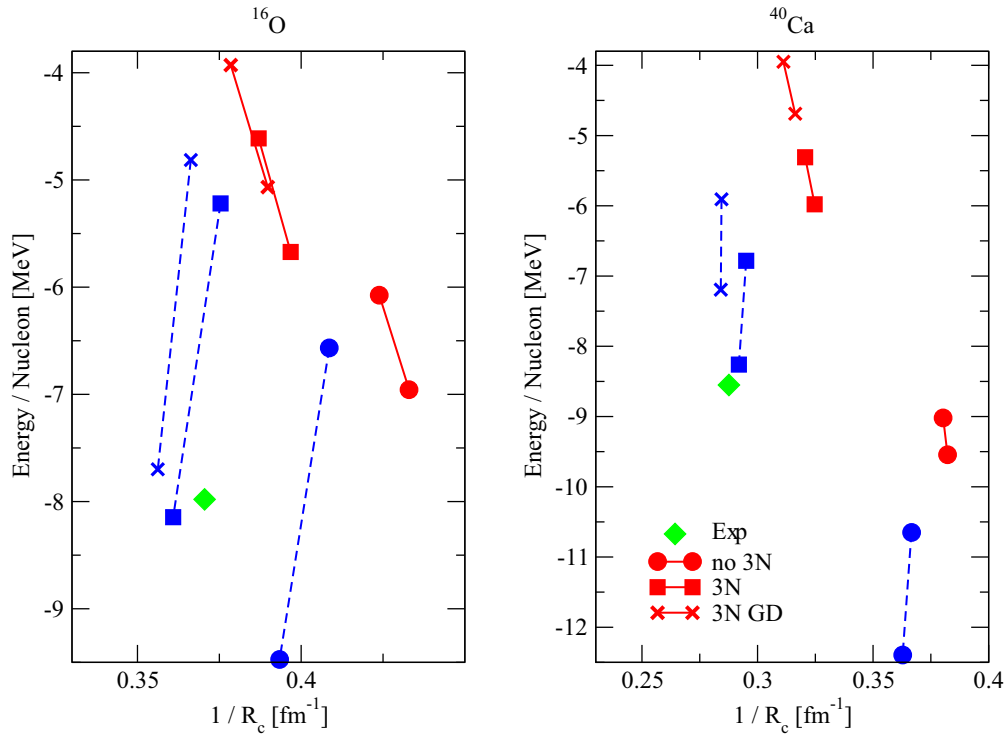

FIG. 3. (Color online) Results for the energy per nucleon and the radius of the charge distribution (R_c) for ^{16}O (left panel) and ^{40}Ca are presented in an energy versus $1/R_c$ plot to enable comparison with the corresponding figures for nuclear matter (Figs. 1 and 2). Results referring to BHF calculations with different values of C in Eq. (10) defining the particle spectrum in the Bethe-Goldstone equation are connected by a red solid line; those of RBHF calculations are connected by a blue dashed line. Results of calculations with just the 2N interaction, with inclusion of the 3N term, and including the 3N term via a global density approximation are visualized by a dot, a box, and a cross, respectively. The experimental result is given in terms of a green diamond symbol.

a lowest eigenvalue of 10 MeV for the $1s0d$ shell. Therefore a shift of $C = 15$ MeV to a single-particle energy of -5 MeV seems plausible to approximate a continuous particle state spectrum. A larger value of C leads to more attraction, and so the lines displayed in Fig. 3 indicate the range of results changing C from 5 to 15 MeV, with the less attractive energy representing the $C = 5$ MeV result. In this figure the results of BHF calculations are represented by symbols connected by a solid red line, while the symbols connected by a dashed blue line refer to the results of RBHF calculations. The remarkable sensitivity of the calculation to these changes in the spectrum of the particle states calls for more sophisticated investigations on this issue, to obtain unambiguous results.

The effects of including the 3N force can be seen by comparing the results visualized in in Fig. 3 in terms of the square boxes with the corresponding results displayed by circles. As expected, the inclusion of the 3N interaction yields a repulsive effect and leads to a reduction of the total energy accompanied by an increase of the nuclear radius. Comparing this effect with the corresponding repulsive effect that one can obtain with a lowering of the parameter C just discussed, one finds that the 3N force yields a larger increase in the radius if the energy is changed by a similar amount. This may reflect the fact that a proper treatment of the 3N force as compared to a modification of the 2N interaction has a larger effect on the single-particle potential [see the discussion in the Introduction connected to Eqs. (3) and (4)]. Therefore a repulsive 3N interaction will be more efficient in changing the single-particle potential and the resulting radius of the particle distribution than in making a similar change in the 2N interaction.

Figure 3 also shows results displayed in terms of crosses and denoted as 3N GD (see also Table I). As discussed above, this approximation scheme describes an attempt to evaluate the effects of the 3N force in nuclear matter at various densities and then transfer the result to the calculation of finite nuclei by choosing the density of nuclear matter to be identical to the average particle density calculated for the nucleus considered. We find that this global density (GD) approximation yields effects which are similar with a tendency to overestimate the corresponding effects of a direct treatment in the finite nucleus by 20 to 30 percent.

Similar calculations have also been done for the nucleus ^{40}Ca. Results on the "saturation properties" of this nucleus are displayed in the right panel of Fig. 3 considering the values $C = 10$ and $C = 15$ MeV for the parametrization of the particle state spectrum. More explicit results on the single−particle energies are shown in Table II assuming $C = 10$ MeV. The main features of these results for ^{40}Ca are very similar to those discussed for the example ^{16}O and therefore confirm these findings.

It is worth noting that, assuming $C = 15$ MeV and including the 3N force, RBHF calculations of both nuclei yield results

TABLE II. Results for ^{40}Ca using BHF and RBHF approximations. The Pauli operator in the Bethe Goldstone equation has been defined in terms of an oscillator function using an oscillator parameter $b = 2.0$ fm, and $C = 10$ MeV has been used to define the single-particle energies in Eq. (10). For further details see the caption of Table I.

	NN only			with 3N			with 3N GD		
	BHF	RBHF		BHF	RBHF		BHF	RBHF	
	ε (MeV)	ε (MeV)	P	ε (MeV)	ε (MeV)	P	ε (MeV)	ε (MeV)	P
	Protons								
$0s_{1/2}$	−94.27	−76.04	0.850	−53.18	−36.65	0.855	−45.35	−31.34	0.790
$p_{3/2}$	−63.36	−48.11	0.869	−34.63	−21.93	9.745	−27.58	−17.92	0.692
$p_{1/2}$	−53.82	−41.61	0.863	−30.53	−19.82	0.723	−24.10	−16.16	0.676
$d_{5/2}$	−33.20	−21.81	0.816	−16.61	−8.47	0.718	−11.36	−5.51	0.724
$1s_{1/2}$	−26.61	−18.06	0.739	−12.88	−7.15	0.726	0.9.33	−5.04	0.743
$d_{3/2}$	−18.22	−12.20	0.736	−10.66	−5.29	0.713	−6.33	−2.85	0.731
	Neutrons								
$s_{1/2}$	−104.3	−83.71	0.854	−61.35	−42.02	0.868	−53.30	−36.39	0.810
$p_{3/2}$	−72.74	−55.31	0.869	−42.44	−27.02	0.760	−35.02	−22.71	0.704
$p_{1/2}$	−63.12	−48.74	0.865	−38.23	−24.84	0.737	−31.41	−20.89	0.687
$d_{5/2}$	−42.16	−28.58	0.830	−23.99	−13.36	0.720	−18.38	−10.13	0.722
$1s_{1/2}$	−34.93	−24.43	0.752	−20.13	−12.00	0.723	−16.26	−9.63	0.736
$d_{3/2}$	−26.88	−18.72	0.749	−17.84	−10.09	0.712	−13.19	−7.39	0.725
E/A (MeV)	−9.02	−10.65		−5.31	−6.78		−3.95	−5.91	
R_c (fm)	2.62	2.72		3.11	3.38		3.21	3.52	

for energy and radius of the charge distribution that are in good agreement with the experimental data (see Fig. 3 and Table III). We do not intent to celebrate this as a success of the Dirac BHF approach, or of the BHF approach simulating the Dirac effects of DBHF in terms of a 3N force. We will keep in mind that the strength of the 3N force, which was motivated to simulate the Dirac effect, has been adjusted to reproduce the saturation point of nuclear matter. With the 3N force adjusted we made a reasonable but not uniquely justified choice for the description of the particle-state spectrum to end up with a good description of the bulk properties of finite nuclei as well.

Nevertheless, this result shows that, using an appropriate 3N force to simulate the effects of Dirac spinors modified in the nuclear medium within the framework of nonrelativistic BHF calculations, one may be able to describe the bulk properties of nuclear matter and finite nuclei based on a realistic NN interaction.

TABLE III. Results for the energy per nucleon E/A and the radius of the charge distribution R_c for ^{16}O and ^{40}Ca calculated in BHF and RBHF approximation are compared to the experimental data [52,53]. In contrast to the calculations leading to the results in table I and table II a shift $C = 15$ MeV has been used to define the single-particle energies in Eq. (10).

		NN only		with 3N		Expt.
		BHF	RBHF	BHF	RBHF	
^{16}O	E/A (MeV)	−6.96	−9.47	−5.67	−8.15	−7.98
	R_c (fm)	2.31	2.54	2.52	2.77	2.70
	E/A (MeV)	−9.54	−12.40	−5.98	−8.26	−8.55
	R_c (fm)	2.62	2.76	3.08	3.43	3.48

The description of bulk properties (energy, radius of particle distribution, density) is important, but it only only one set of features of nuclear structure that we hope to describe within the relativistic DBHF approach. Other important aspects we hope to describe within a relativistic description of nuclear systems are the energy dependence of the optical potential [54] and the spin-orbit splitting of the single-particle energies [55], which is enhanced due to the enhancement of the small component of Dirac spinors in the nuclear medium.

Is this enhancement of the spin-orbit splitting, which is important to describe the strength of the spin-orbit term observed in the experiment, also simulated by the simple 3N force of Eq. (1)? Inspecting, e.g., the single-particle energies of the $p_{3/2}$ and $p_{1/2}$ states listed in Table I we do not find an enhancement of the spin-orbit splitting with the 3N force included. In fact, the differences between these single-particle energies are always smaller with inclusion of the 3N force. This is related to the fact that the 3N force yields larger values for the radii which reduces the spacing between the single-particle states. But even if one accounts for this size effect, the 3N force does not provide an enhancement of the spin-orbit splitting. This could be achieved by introducing an appropriate spin structure in the 3N force, a feature which presumably would lead to more parameters and spoil the simplicity of the present approach.

IV. CONCLUSION

An attempt has been made to simulate the relativistic features of the Dirac-Brueckner-Hartree-Fock (DBHF) approach by adding effects of a simple three-nucleon (3N) force to nonrelativistic many-body calculations based on the BHF approach. One parameter, the strength of the 3N force, is adjusted to reproduce the empirical saturation point

of infinite nuclear matter and is then used without further modifications for the description of finite nuclei. Special attention is paid to the energy spectrum of particle states, which is used in the propagator of the Bethe-Goldstone equation, and the importance of rearrangement terms due to the energy dependence of the effective interaction. For the studies of finite nuclei in particular, more effort is needed to optimize the treatment of the propagator in the Bethe-Goldstone equation. Taking a reasonable choice for the particle state spectrum and including the effects of rearrangement terms, the renormalized Brueckner-Hartree-Fock calculations with 3N force can reproduce the empirical values for the energy and radius of charge distribution of nuclei such as ^{16}O and ^{40}Ca. This attempt to simulate the effects of the relativistic features of the DBHF approach, however, fails to reproduce other predictions of the Dirac phenomenology such as the strength of the spin-orbit term in the single-particle field.

ACKNOWLEDGMENTS

This work has been performed as a part of a project (Mu 705/10-1) supported by the Deutsche Forschungsgemeinschaft, DFG.

[1] T. H. R. Skyrme, Nucl. Phys. **9**, 615 (1959).
[2] J. Sadoudi, T. Duguet, J. Meyer, and M. Bender, Phys. Rev. C **88**, 064326 (2013).
[3] B. D. Serot and J. D. Walecka, Adv. Nucl. Phys. **16**, 1 (1986).
[4] R. Machleidt, Adv. Nucl. Phys. **19**, 189 (1989).
[5] R. B. Wiringa, V. G. J. Stoks, and R. Schiavilla, Phys. Rev. C **51**, 38 (1995).
[6] R. Machleidt, F. Sammarruca, and Y. Song, Phys. Rev. C **53**, R1483 (1996).
[7] H. Müther and A. Polls, Prog. Part and Nucl. Phys. **45**, 243 (2000).
[8] K. T. R. Davies, R. J. McCarthy, J. W. Negele, and P. U. Sauer, Phys. Rev. C **10**, 2607 (1974).
[9] R. K. Tripathi, A. Faessler, and H. Müther, Phys. Rev. C **10**, 2080 (1974).
[10] K. T. R. Davies and R. J. McCarty, Phys. Rev. C **4**, 81 (1971).
[11] W. Zuo, I. Bombaci, and U. Lombardo, Phys. Rev. C **60**, 024605 (1999).
[12] G. Baym and L. P. Kadanov, Phys. Rev. **124**, 287 (1961).
[13] F. Coester, S. Cohen, B. D. Day, and C. M. Vincent, Phys. Rev. C **1**, 769 (1970).
[14] K. Holinde, Phys. Rep. **68**, 121 (1981).
[15] R. B. Wiringa, R. A. Smith, and T. L. Ainsworth, Phys. Rev. C **29**, 1207 (1984).
[16] M. R. Anastasio, H. Müther, A. Faessler, K. Holinde, and R. Machleidt, Phys. Rev. C **18**, 2416 (1978).
[17] A. Faessler, H. Müther, K. Shimizu, and W. Wadia, Nucl. Phys. A **333**, 428 (1980).
[18] R. Brockmann and R. Machleidt, Phys. Rev. C **42**, 1965 (1990).
[19] R. Fritz, H. Müther, and R. Machleidt, Phys. Rev. Lett. **71**, 46 (1993).
[20] G. E. Brown, W. Weise, G. Baym, and J. Speth, Comments Nucl. Part. Phys. **17**, 39 (1987).
[21] A. Bouyssy, J.-F. Mathiot, N. Van Giai, and S. Marcos, Phys. Rev. C **36**, 380 (1987).
[22] M. R. Anastasio, L. S. Celenza, W. S. Pong, and C. M. Shakin, Phys. Rep. **100**, 327 (1983).
[23] C. J. Horowitz and B. D. Serot, Nucl. Phys. A **464**, 613 (1987).
[24] B. ter Haar and R. Malfliet, Phys. Rep. **149**, 207 (1987).
[25] F. de Jong and H. Lenske, Phys. Rev. C **58**, 890 (1998).
[26] T. Gross-Boelting, C. Fuchs, and Amand Faessler, Nucl. Phys. A **648**, 105 (1999).
[27] D. Alonso and F. Sammarruca, Phys. Rev. C **67**, 054301 (2003).
[28] E. N. E. van Dalen and H. Müther, Int. J. Mod. Phys. E **19**, 2077 (2010).
[29] N. van Giai, B. V. Carlson, Z. Ma, and H. H. Wolter, J. Phys. G **37**, 064043 (2010).
[30] E. N. E. van Dalen and H. Müther, Phys. Rev. C **84**, 024320 (2011).
[31] C. Fuchs, H. Lenske, and H. H. Wolter, Phys. Rev. C **52**, 3043 (1995).
[32] H. Müther, R. Machleidt, and R. Brockmann, Phys. Rev. C **42**, 1981 (1990).
[33] J. Carlson, V. R. Pandharipande, and R. Wiringa, Nucl. Phys. A **401**, 59 (1983).
[34] M. Baldo and L. S. Ferreira, Phys. Rev. C **59**, 682 (1999).
[35] P. Grange, A. Lejeune, M. Martzolff, and J.-F. Mathiot, Phys. Rev. C **40**, 1040 (1989).
[36] V. Soma and P. Bożek, Phys. Rev. C **78**, 054003 (2008).
[37] K. Hebeler and A. Schwenk, Phys. Rev. C **82**, 014314 (2010).
[38] A. Carbone, A. Polls, and A. Rios, Phys. Rev. C **88**, 044302 (2013).
[39] D. S. Koltun, Phys. Rev. Lett. **28**, 182 (1972).
[40] H. Q. Song, M. Baldo, G. Giansiracusa, and U. Lombardo, Phys. Rev. Lett. **81**, 1584 (1998).
[41] J. P. Jeukenne, A. Lejeunne, and C. Mahaux, Phys. Rep. **25**, 83 (1976).
[42] E. Schiller, H. Müther, and P. Czerski, Phys. Rev. C **59**, 2934 (1999); **60**, 059901(E) (1999).
[43] K. Suzuki, R. Okamoto, M. Kohno, and S. Nagata, Nucl. Phys. A **150**, 467 (1970).
[44] P. U. Sauer, Nucl. Phys. A **665**, 92 (2000).
[45] H. Müther and P. U. Sauer, *Computational Nuclear Physics 2*, (Springer Verlag, N. Y., 1993), p. 30.
[46] A. Faessler, T. T. S. Kuo, and H. Müther, Z. Physik A **294**, 95 (1980).
[47] C. Mahaux and R. Sartor, Adv. Nucl. Phys. **20**, 1 (1991).
[48] Kh. S. A. Hassaneen and H. Müther, Phys. Rev. C **70**, 054308 (2004).
[49] W. Zuo, U. Lombardo, and H.-J. Schulze, Phys. Lett. B **432**, 241 (1998).
[50] W. Zuo, U. Lombardo, H.-J. Schulze, and Z. H. Li, Phys. Rev. C **74**, 014317 (2006).
[51] J. G. Zabolitzky, Phys. Lett. B **47**, 487 (1973).
[52] Atomic Mass Data of National Nuclear Data Center, Brookhaven National Laboratory, www.nndc.bnl.gov
[53] I. Angeli and K. P. Marinova, At. Data Nuc. Data Tables **99**, 69 (2013).
[54] Ruirui Xu, Zhongyu Ma, E. N. E. van Dalen, and H. Müther, Phys. Rev. C **85**, 034613 (2012).
[55] L. Zamick, D. C. Zheng, and H. Müther, Phys. Rev. C **45**, 2763 (1992).